DOI: 10.1002/chem.201100751

X-ray and Solution Structures of Cu^{II}GHK and Cu^{II}DAHK Complexes: Influence on Their Redox Properties**

Christelle Hureau,*[b] Hélène Eury,[b] Régis Guillot,[c] Christian Bijani,[b] Stéphanie Sayen,[d] Pier-Lorenzo Solari,[e] Emmanuel Guillon,[d] Peter Faller,[b] and Pierre Dorlet*[a]

Abstract: The Gly-His-Lys (GHK) peptide and the Asp-Ala-His-Lys (DAHK) sequences are naturally occurring high-affinity copper(II) chelators found in the blood plasma and are hence of biological interest. A structural study of the copper complexes of these peptides was conducted in the solid state and in solution by determining their X-ray structures, and by using a large range of spectroscopies, including EPR and HYSCORE (hyperfine sub-level correlation), X-ray absorption and ^{1}H and ^{13}C NMR spectroscopy. The results indicate that the structures of [Cu^{II}(DAHK)] in the solid state and in solution are similar and confirm the equatorial coordination sphere of NH_2, two amidyl N and one imidazole N. Additionally, a water molecule is bound apically to Cu^{II} as revealed by the X-ray structure. As reported previously in the literature, [Cu^{II}(GHK)], which exhibits a dimeric structure in the solid state, forms a monomeric complex in solution with three nitrogen ligands: NH_2, amidyl and imidazole. The fourth equatorial site is occupied by a labile oxygen atom from a carboxylate ligand in the solid state. We probe that fourth position and study ternary complexes of [Cu^{II}(GHK)] with glycine or histidine. The Cu^{II} exchange reaction between different DAHK peptides is very slow, in contrast to [Cu^{II}-(GHK)], in which the fast exchange was attributed to the presence of a [$Cu^{II}(GHK)_2$] complex. The redox properties of [Cu^{II}(GHK)] and [Cu^{II}-(DAHK)] were investigated by cyclic voltammetry and by measuring the ascorbate oxidation in the presence of molecular oxygen. The measurements indicate that both Cu^{II} complexes are inert under moderate redox potentials. In contrast to [Cu^{II}(DAHK)], [Cu^{II}-(GHK)] could be reduced to Cu^{I} around −0.62 V (versus AgCl/Ag) with subsequent release of the Cu ion. These complete analyses of structure and redox activity of those complexes gave new insights with biological impact and can serve as models for other more complicated Cu^{II}–peptide interactions.

Keywords: bioinorganic chemistry · copper · ligand interactions · peptides · structural characterisation

Introduction

Copper is an essential trace element involved in the activities of many enzymes and proteins but can become toxic if its homeostasis is not tightly controlled. Pathologies related to copper include Menkes and Wilson diseases and neurodegenerative disorders such as Alzheimer's or Prion diseases. In the latter, the redox activity of copper seems to play a crucial role.[1] The Gly-His-Lys (GHK) peptide and the Asp-Ala-His-Lys (DAHK) sequence are naturally occurring high-affinity copper chelators found in the blood plasma.[2] GHK was isolated by Pickart et al.[3] and first described as a

[a] Dr. P. Dorlet
Laboratoire du Stress Oxydant et Détoxication
CNRS, URA 2096, 91191 Gif-sur-Yvette (France)
and
CEA, iBiTec-S, SB²SM, 91191 Gif-sur-Yvette (France)
Fax: (+33) 1-69-08-87-17
E-mail: pierre.dorlet@cea.fr

[b] Dr. C. Hureau, H. Eury, Dr. C. Bijani, Prof. P. Faller
CNRS, LCC (Laboratoire de Chimie de Coordination)
205, route de Narbonne, 31077 Toulouse (France)
and
Université de Toulouse; UPS, INPT
LCC, 31077 Toulouse (France)
Fax: (+33) 5-61-55-30-03
E-mail: hureau@lcc-toulouse.fr

[c] Dr. R. Guillot
CNRS, ICMMO—UMR 8182, Bât. 420
Université Paris-Sud 11, 91405 Orsay Cedex (France)

[d] Dr. S. Sayen, Prof. E. Guillon
Groupe de Chimie de Coordination, CNRS
ICMR—UMR 6229
Université de Reims Champagne-Ardenne
51687 Reims Cedex 2 (France)

[e] Dr. P.-L. Solari
Synchrotron SOLEIL, Saint-Aubin
91192 Gif-Sur-Yvette Cedex (France)

[**] GHK and DAHK refers to the peptide chains Gly-His-Lys and Asp-Ala-His-Lys, respectively.

Supporting information for this article is available on the WWW under http://dx.doi.org/10.1002/chem.201100751.

liver cell growth factor. Further studies showed that GHK possesses a wide range of biological activities, including acceleration of wound healing[4] and tissue remodelling.[5] When complexed to this peptide, Cu^{II} is bound by the $-NH_2$, the N^{π} of the histidine residues and one amidyl group from the backbone. The equatorial coordination plane is completed in solution by a labile ligand, thus allowing formation of ternary species with exogenous amino acid residues in a biological medium.[6] DAHK is the N-terminal fragment of the human serum albumin (HSA). HSA is the most abundant blood serum protein involved in Cu^{II} transport[7] and also a major component of cerebrospinal fluid. Among the two Cu^{II} binding sites present in HSA, the N-terminal motif possesses the higher affinity.[8] Cu^{II} is bound to the $-NH_2$, the N^{π} of the histidine residues and two amidyl groups from the peptide backbone, thus being archetypal of the so-called ATCUN binding motif (H_2N-XXH beginning sequence in a peptide/protein) also found in other proteins, that is, neuromedins C and K, human sperm protamine P2a and histatins.[2a] DAHK has also recently been shown to restore cell survival of cells exposed to Cu and Cu-Aβ (Aβ is the amyloid-β peptide involved in Alzheimer's disease) and this effect has been attributed to redox silencing of Cu when bound to DAHK.

As a consequence, Cu^{II} binding to these two peptides is of paramount importance. In addition, the present study was also motivated by the need to obtain a set of reference spectroscopic signatures coupled to redox behaviour to model in detail Cu^{II} sites with 3N+1O or 4N equatorial binding modes in other peptides and proteins. In this paper, we give new insights into the Cu^{II} coordination to the DAHK and GHK peptides and discuss the results in comparison with studies previously performed on these species. The X-ray structures of both complexes are described and their solution structures are characterised by advanced spectroscopic methods. The redox properties are then analysed and detailed in relation to the structural observations.

Results and Discussion

X-ray structures: The crystal structures of the [Cu^{II}(GHK)] and [Cu^{II}(DAHK)] complexes were determined by single-crystal X-ray diffraction. Table 1 and Table 2 summarise crystal data and selected bond lengths and angles. In both cases, the Cu^{II} ion is penta-coordinated in a distorted square-planar pyramid environment with an oxygen in the apical position.

In the case of [Cu^{II}(GHK)] (see Figure 1), the structure is essentially identical to that previously reported by Perkins and co-workers,[9] and close to that of [Cu^{II}(GH)].[10] The binding mode in the equatorial plane is 3N+1O: the Cu^{II} ion is ligated by the glycine amino nitrogen, the deprotonated amide nitrogen of the glycine–histidine peptide bond, the N^{π} nitrogen of the imidazole side chain of the histidine and the lysine carboxylate of a neighbouring complex. The apical oxygen is provided also by the lysine carboxylate of another neighbouring complex. This is in contrast with the structure of [Cu^{II}(GH)][10] for which the apical oxygen is a water molecule. Two [Cu^{II}(GHK)] monomeric units are thus arranged in a dimeric diamond-core type structure in which the two Cu^{II} centres are spaced by 3.458 Å and the two bridging oxygen atoms by 2.874 Å. A total of 16 sites for a

Table 1. Crystal data and structure refinement for [Cu^{II}(GHK)] and [Cu^{II}(DAHK)].

	[Cu^{II}(DAHK)]	[Cu^{II}(GHK)]
formula	$C_{19}H_{30}CuN_7O_7\cdot 7H_2O\cdot Cl$	$C_{14}H_{23}CuN_6O_4\cdot 9.25H_2O$
M_r [g mol^{-1}]	693.61	550.92
T [K]	100(1)	100(1)
λ [Å]	0.71073	0.71073
crystal size [mm^3]	0.18×0.06×0.01	0.32×0.27×0.21
crystal colour	purple	blue
crystal system	trigonal	tetragonal
space group	$P3_2$	$P4_12_12$
unit cell dimensions	0.18×0.06×0.01	0.32×0.27×0.21
a [Å]	14.4934(3)	14.4793(2)
b [Å]	14.4934(3)	14.4793(2)
c [Å]	12.1728(5)	26.3306(7)
α [°]	90	90
β [°]	90	90
γ [°]	120	90
V [Å^3]	2214.43(11)	5520.21(18)
Z	3	8
ρ_{calcd} [Mg m^{-3}]	1.560	1.326
absorption coefficient [mm^{-1}]	0.907	0.856
F(000)	1095	2272
reflns collected	8978	115905
indep reflns (R_{int})	5001 (0.0631)	8484 (0.0391)
obsd reflns ($I>2\sigma(I)$)	7423	7094
final R indices ($I>2\sigma(I)$)	$R1=0.0457$, $wR2=0.1017$	$R1=0.0666$, $wR2=0.1899$
R indices (all data)	$R1=0.0645$, $wR2=0.1110$	$R1=0.0854$, $wR2=0.2267$
Flack parameter	0.005(10)	0.022(19)
S	1.069	1.060
$(\Delta/\sigma)_{max}$	0.000	0.009
$(\Delta\rho)_{max/min}$ [e Å^{-3}]	0.981/−0.728	0.780/−0.137

Table 2. Selected bond lengths [Å] and angles [°].

[Cu^{II}(DAHK)] (100 K)		[Cu^{II}(GHK)] (100 K)	
Cu–N(1)	2.029(3)	Cu–N(1)	1.957(4)
Cu–N(2)	1.906(3)	Cu–N(2)	1.945(3)
Cu–N(3)	1.967(2)	Cu–N(3)	2.003(3)
Cu–N(4)	1.969(3)	Cu–O(3)[a]	1.967(2)
Cu–O(8)	2.565(3)	Cu–O(3)[b]	2.513(3)
N(1)-Cu-N(2)	83.70(11)	N(1)-Cu-N(2)	93.58(15)
N(1)-Cu-N(3)	166.74(10)	N(1)-Cu-N(3)	172.79(16)
N(1)-Cu-N(4)	98.81(11)	N(1)-Cu-O(3)[a]	90.40(15)
N(1)-Cu-O(8)	90.28(11)	N(1)-Cu-O(3)[b]	98.50(14)
N(2)-Cu-N(3)	83.11(11)	N(2)-Cu-N(3)	83.53(12)
N(2)-Cu-N(4)	173.55(10)	N(2)-Cu-O(3)[a]	175.82(12)
N(2)-Cu-O(8)	89.98(11)	N(2)-Cu-O(3)[b]	99.34(12)
N(3)-Cu-N(4)	94.45(11)	N(3)-Cu-O(3)[a]	92.67(12)
N(3)-Cu-O(8)	88.34(11)	N(3)-Cu-O(3)[b]	88.51(15)
N(4)-Cu-O(8)	95.89(11)	O(3)[a]-Cu-O(3)[b]	78.75(16)

[a] Symmetry code: $^1/_2-x$, y, $^1/_2-z$. [b] Symmetry code: $^1/_2-y$, $^1/_2+x$, $^1/_4+z$.

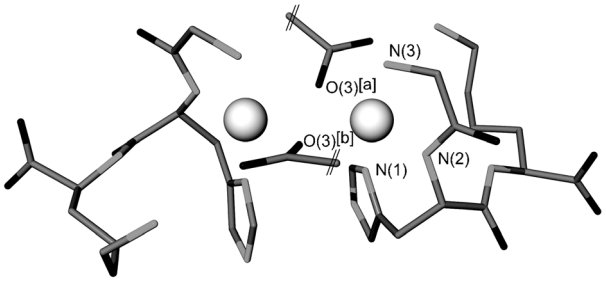

Figure 1. X-ray structure of the [Cu^{II}(GHK)] complex. Each Cu^{II} ion is penta-coordinated. Considering the ion on the right, the equatorial positions are occupied by atoms N(1) to N(3) and $O(3)^{[a]}$, whereas the apical position is occupied by $O(3)^{[b]}$. These last two oxygen atoms are shared with the other Cu^{II} ion for which their position is interchanged ($O(3)^{[a]}$ being in the apical position, whereas $O(3)^{[b]}$ is in the equatorial position for the ion on the left).

water molecule were present in the unit cell of our structure of [Cu^{II}(GHK)] with an occupancy of 9.25 compared with 14 sites for the structure of Perkins et al. with an occupancy of 9.2.

The complex [Cu^{II}(DAHK)] corresponds to the high-affinity binding site of human serum albumin and its crystal structure is reported here for the first time (see Figure 2).

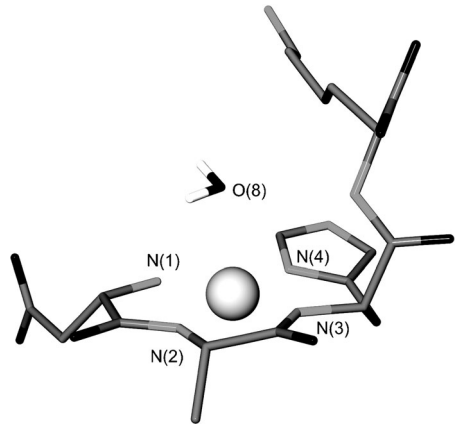

Figure 2. X-ray structure of the [Cu^{II}(DAHK)] complex. The Cu^{II} ion is penta-coordinated with four nitrogen ligands in equatorial positions (N(1) to N(4)) and one water molecule in the apical position (O(8)).

The Cu^{II} ion is bound by 4 nitrogen ligands in the equatorial plane: the aspartate amino group, two deprotonated amide functions from the first two peptide bonds and the N^{π} nitrogen of the imidazole side chain of the histidine residue. The apical oxygen along the Jahn–Teller distortion axis is provided by a water molecule in hydrogen-bond interactions with other solvent molecules in the unit cell. By contrast with the structure of [Cu^{II}(GHK)], all protons could be resolved and refined in this structure. The peptide is in its fully protonated form and one chloride counterion per complex is present. In addition, the crystal structure of this complex is monomeric rather than the dinuclear motif observed for [Cu^{II}-(GHK)]. A total of 7 water molecules are present in the unit cell. The main difference with the X-ray structure of Cu^{II} bound to GGH–NH_2, the simplest peptide to form an ATCUN motif, is the presence of an apical water only in one out of two complexes in the [Cu^{II}(GGH–NH_2)] structure.[11] Contrary to what has been conjectured previously,[11,12] the carboxyl oxygen from Asp1 does not occupy the apical position in the [Cu^{II}(DAHK)] complex.

Electronic and ESI-MS data: In solution and at room temperature, the characteristic blue and purple colours for [Cu^{II}(GHK)] and [Cu^{II}(DAHK)] are retained (see Figure S1 in the Supporting Information for UV/Vis and circular dichroism data). The ESI-MS spectra (positive detection mode) of [Cu^{II}(GHK)] and [Cu^{II}(DAHK)] are shown in Figure 3 and Figure S2 in the Supporting Information. Peaks

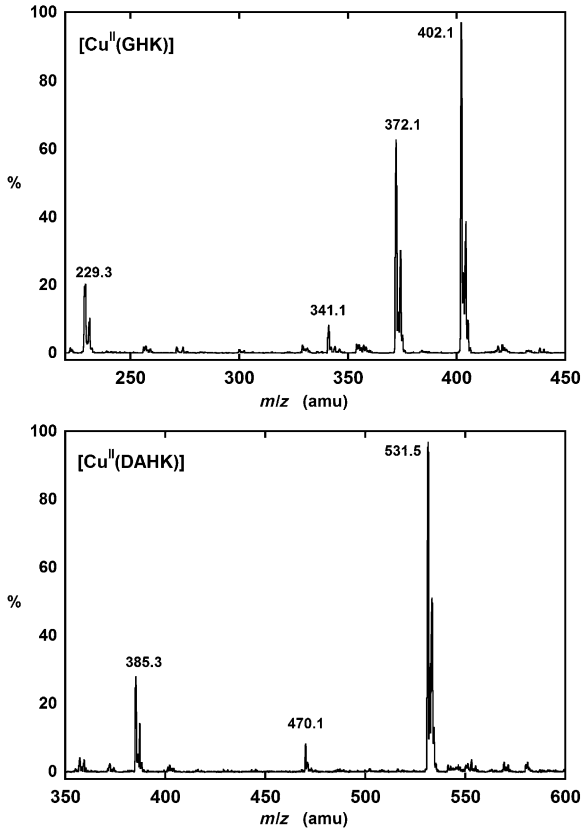

Figure 3. ESI-MS spectra of [Cu^{II}(GHK)] and [Cu^{II}(DAHK)] complexes in the positive detection mode. [Cu^{II}(peptide)] = 200 μM, pH 7.6 (adjusted with NH_3).

of Cu^{II}-containing species are recognizable by their isotopic pattern ($^{63}Cu = 65\%$, $^{65}Cu = 35\%$). The main peak at m/z 531.5 in the [Cu^{II}(DAHK)] spectrum (100% of relative intensity) corresponds to the two-proton adduct of the once negatively charged [Cu^{II}(DAHK)] species. This was confirmed by the detection of a peak at m/z 529.5 in the negative detection mode (data not shown). Another peak detected at m/z 385.3 (30% of relative intensity) is attributed to the [Cu^{II}(DAH)] species issued from the fragmentation of

the parent peak at *m*/*z* 531.5. Departure of the Lys residues from the [Cu^{II}(DAHK)] complex is in line with a Cu^{II} binding site in which only the first three residues are involved. The main peak detected in the [Cu^{II}(GHK)] spectrum corresponds to the monocationic [Cu^{II}(GHK)] species. A peak at *m*/*z* 803.5 that corresponds to the [Cu_2(GHK)$_2$] species (Figure S2) is observed but with a very low relative intensity (less than 5%), thereby suggesting that the binuclear unit observed in the solid state is mainly disrupted in solution. Fragmentation peaks observed at *m*/*z* 372.1 (65% of relative intensity) and 229.3 (22% of relative intensity) are attributed to the departure of the [NH_2–CH_2] N-terminal motif and the additional removal of the Lys residues from the parent species and were confirmed by MS/MS experiments. Contrary to what was observed in the case of [Cu^{II}(DAHK)], the main fragmentation peak observed corresponds to the removal of the [NH_2–CH_2] N-terminal motif suggesting that the principal Cu^{II} anchor site is the His residue. Only in a second time, the Lys residue is lost. The very low intensity of the peaks observed at *m*/*z* 470.1 ([Cu^{II}(DAHK)] spectrum) and at *m*/*z* 341.1 ([Cu^{II}(GHK)] spectrum), which correspond to the DAHK and GHK ligands, respectively, agrees with a Cu^{II} ion strongly bound by both peptides.

X-ray absorption spectroscopy (XAS): To gain further insight into Cu^{II} coordination in solution, X-ray absorption spectra were analysed in the near-edge structure (XANES) and in the extended region (EXAFS). EXAFS data (Figure S3 in the Supporting Information) are best fitted with five N/O neighbours ([Cu^{II}(GHK)]) and with either five or six N/O neighbours ([Cu^{II}(DAHK)]), four of them being significantly closer (Table 3). In the case of [Cu^{II}(DAHK)], it is difficult to determine precisely whether one or two axial oxygen atoms are involved in the copper coordination in solution, given both fits were very similar as shown by the very close value of the goodness-of-fit (0.44 and 0.53% for (4+2) and (4+1) neighbours, respectively).

The EXAFS data are thus consistent with the X-ray structures. Qualitative XANES analysis agrees with geometrical data determined by EXAFS. The [Cu^{II}(DAHK)] and [Cu^{II}-(GHK)] XANES data (Figure 4) show the presence of the pre-edge P peak at 8979.7 eV, assigned to the 1s→3d transition characteristic of the Cu^{II} valence state. The lower intensity of the [Cu^{II}(DAHK)] pre-edge feature indicates that the Cu^{II} centre is in a more centro-symmetric environment than in [Cu^{II}(GHK)].[13] The XANES signatures differ between the two Cu^{II} species, as indicated by more intense B and D peaks and less-pronounced A and C peaks for [Cu^{II}(GHK)] than [Cu^{II}(DAHK)]. In related systems, these peaks have been proposed to be sensitive to second- and third-shell perturbations.[14] More precisely, an increase of the B peak and a decrease of the C peak were related to a more important contribution of external shells. In the present case, the more intense B peak (or less intense C peak) for [Cu^{II}(GHK)] relative to [Cu^{II}(DAHK)] is likely related to the possibility of having an exchangeable fourth equatorial ligand in the [Cu^{II}(GHK)] species, also consistent with a greater Debye–Waller factor. These results show that the square pyramidal structure observed in the solid state for the two complexes is retained in solution.

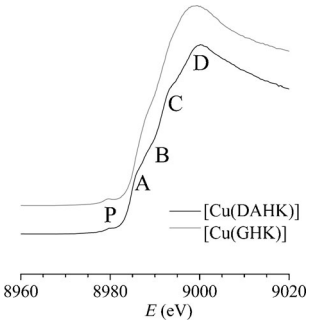

Figure 4. The XANES regions of the normalized absorption amplitude versus energy for [Cu^{II}(DAHK)] and [Cu^{II}(GHK)] complexes at pH 7.4. [Cu^{II}(GHK)] = 50 mM and [Cu^{II}(DAHK)] = 50 mM, T = 298 K.

EPR spectroscopy: EPR spectra (9 GHz) were recorded for [Cu^{II}(GHK)] and [Cu^{II}(DAHK)] complexes in solution and are shown in Figure 5. Characteristic parameters are listed in Table 4. Both complexes display a classical mononuclear square-planar-type EPR spectrum with some resolved superhyperfine interaction in the $g_\perp$ region, as previously reported.[15] The $g_\parallel$ and $A_\parallel$ values measured on the spectra are consistent with the 3N+1O and 4N binding mode, respectively.[16] These binding modes are thus retained from the solid state to solution. In the case of [Cu^{II}(GHK)], however, the dinuclear structure observed in the crystal state is not present in solution.[15a] Therefore it is likely that the equatorial oxygen ligand, provided by the C-terminus carboxylate

Table 3. First coordination shell structural data obtained from *R* space fits of EXAFS spectra: *N* is the number of neighbours, *R* is the absorber–neighbour distance, σ is the Debye–Waller factor; uncertainties are estimated in coordination numbers to ±10%, in *R* to ±0.02 Å, and to ±0.001 Å^2 in σ^2. For [Cu^{II}(DAHK)], results of fits with 4+2 neighbours and 4+1 neighbours as starting parameters are given.

	Scattered/Backscattered	*N*	*R* [Å]	σ^2 [Å^2]	*R* factor [%][a]
[Cu^{II}(GHK)]	Cu–N/O	4.49	1.97	0.0057	0.12
	Cu–O	0.79	2.61	0.01[b]	
[Cu^{II}(DAHK)]	Cu–N/O	4.49	1.95	0.0046	0.44
(4+2)	Cu–O	1.52	2.50	0.01[b]	
[Cu^{II}(DAHK)]	Cu–N/O	4.42	1.95	0.0045	0.53
(4+1)	Cu–O	1.49	2.49	0.01[b]	

[a] *R* factor represents the overall goodness-of-fit. [b] Fixed parameter.

Table 4. EPR parameters obtained from the spectra of the different complexes in Figure 5.

	$g_\parallel$	$g_\perp$	$A_\parallel$ (^{63}Cu) [MHz]
[Cu^{II}(DAHK)]	2.19	2.04	596
[Cu^{II}(GHK)]	2.23	2.05	560
[Cu^{II}(GHK)$_2$]	2.22	2.05	595
[Cu^{II}(GHK)G]	2.22	2.05	568
[Cu^{II}(GHK)H]	2.21	2.05	590

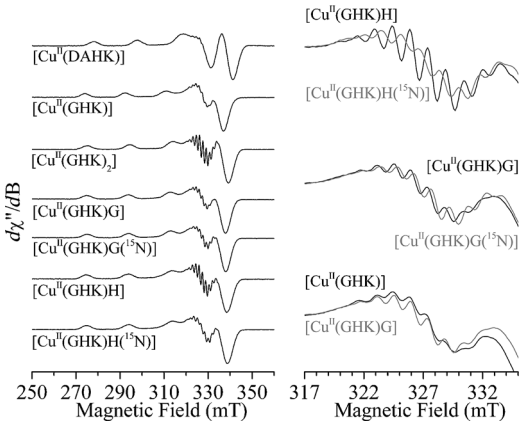

Figure 5. cw EPR spectra recorded for different Cu complexes. The right panel is an enlargement of the $g_\perp$ region for some spectra to compare their superhyperfine patterns. Experimental conditions: microwave frequency 9.42 GHz, microwave power 0.13 mW, modulation amplitude 0.5 mT, modulation frequency 100 kHz, time constant 164 ms, $T=50$ K. Samples prepared in HEPES buffer 100 mM, pH 7.4.

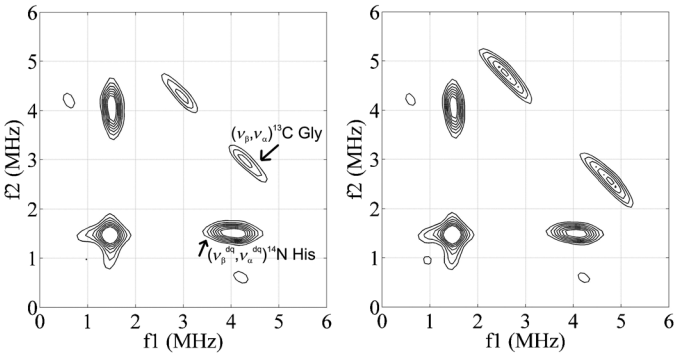

Figure 6. Six-pulse HYSCORE contour plot recorded for [Cu^{II}(GHK)G-(^{13}COO)] (left panel) and [Cu^{II}(GHK)G($^{13}C_\alpha$)] (right panel). The labels for the cross-peaks are indicated on the left panel. Experimental conditions: microwave frequency 9.71 GHz, $B=337$ mT, $\tau_1=104$ ns, $\tau_1=136$ ns, $T=4.2$ K. Samples prepared in HEPES buffer 100 mM, pH 7.4.

of a neighbouring molecule in the crystal, is replaced by a solvent molecule in solution, as previously proposed,[15a] or by an acetate anion present from the peptide batch, sold as an acetate salt. This is in line with the XANES results, which propose an exchangeable equatorial ligand. This labile position has been investigated by addition of either glycine or histidine to the [Cu^{II}(GHK)] solution.

The EPR spectrum obtained for [Cu^{II}(GHK)G] differs slightly from that of [Cu^{II}(GHK)], particularly in the $g_\parallel$ region. The superhyperfine structure on the $g_\perp$ region is also affected. To better probe the coordination mode of the additional glycine amino acid, we have used different isotopically labelled glycine (^{15}N on the amine group or ^{13}C either on the carboxylate group or on the C_α). The superhyperfine structure observed for the ^{15}N-labelled glycine differs sufficiently from that of the unlabelled sample to support binding through the amine function. The weak ^{13}C couplings were probed with pulse EPR. Figure 6 shows the 6-pulse hyperfine sub-level correlation (HYSCORE) contour plots obtained for both carboxylate and C_α-labelled samples. This technique is best adapted in this type of multinuclear coupled systems and was chosen in particular to avoid intensity suppression effects.[17] Ridges centred at the ^{13}C Larmor frequency were detected in both samples. The signal was more intense and the coupling stronger for the C_α-labelled sample relative to the carboxylate-labelled sample, thereby supporting the fact that the additional glycine binds predominantly by its amine function in equatorial position (we note that based on these data we cannot fully exclude that a fraction of the additional glycine binds through its carboxylate function). This binding mode is in agreement with the observations made on the continuous-wave (cw) EPR spectra.

In the case of the [Cu^{II}(GHK)H] complex, a drastic change was observed in the superhyperfine coupling pattern. The seven superhyperfine lines, consistent with a 3N+1O binding mode for [Cu^{II}(GHK)], were replaced by a nine-line pattern consistent with a 4N binding mode for [Cu^{II}-(GHK)H]. This latter pattern is affected when histidine labelled with ^{15}N only on the imidazole ring is used to prepare the complex, thereby indicating that the additional histidine binds to the Cu ion through the imidazole ring rather than its N terminus. This is confirmed by HYSCORE measurements performed on the labelled sample for which a characteristic ^{15}N cross-peak was detected (see Figure S4 in the Supporting Information).

In the case of the [Cu^{II}(GHK)$_2$] complex, a change similar to that observed for the [Cu^{II}(GHK)H] complex was detected in the superhyperfine coupling pattern as well as in the $g_\parallel$ and $A_\parallel$ parameters. This indicates that the second GHK ligand should bind the Cu^{II} centre through its imidazole ring.

NMR spectroscopy: In conjunction with other spectroscopic techniques, NMR spectroscopy can yield information about both Cu^{II} coordination to peptides and the dynamic/mechanism of Cu^{II} exchange between peptides. Due to its paramagnetism, Cu^{II} induces the broadening of the binding groups in its close vicinity.[18] The impact of Cu^{II} on the spectrum will vary considerably depending on the Cu^{II} exchange rate (between holo and apo forms) relative to the timescale of the NMR spectroscopic experiment performed. The two examples studied here are representative of extreme cases: the Cu^{II} exchange is very slow when bound to DAHK and fast when bound to GHK. ^{13}C spectra of the GHK and DAHK peptides in presence of 0.1 and 0.5 equiv of Cu^{II}, respectively, are shown in Figure 7 and Figure 8. The corresponding ^{1}H spectra are shown in the Supporting Information. Based on these data, a mapping of the residues most affected is proposed in Scheme 1.

In the case of the [Cu^{II}(DAHK)] complex, the C- and N-terminal and the side chain of His and Asp are affected, whereas in the [Cu^{II}(GHK)] complex, despite being recorded in the presence of a fivefold lesser Cu^{II} content, almost all residues are strongly broadened with the exception of the Lys side chain. This suggests that in the case of DAHK,

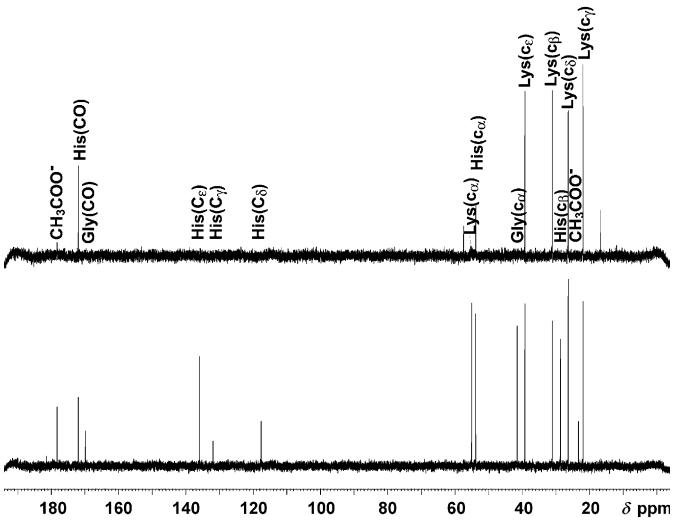

Figure 7. $^{13}C\{^1H\}$ NMR spectra of 10 mM GHK peptide in D_2O in the absence (bottom spectrum) or in the presence of 0.1 equiv Cu^{II} (top spectrum) at pH 7.2. Note that the shift of some peaks is due to a slight modification of the pH value after Cu^{II} addition. $T = 298$ K, $\nu = 125.8$ MHz.

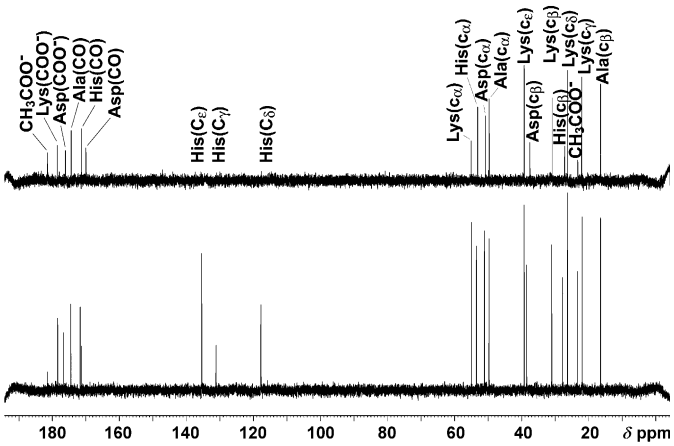

Figure 8. $^{13}C\{^1H\}$ NMR spectra of 10 mM DAHK peptide in D_2O in the absence (bottom spectrum) or in the presence of 0.5 equiv Cu^{II} (top spectrum) at pH 7.2. Note that the shift of some peaks is due to slight modification of the pH value after Cu^{II} addition. $T = 298$ K, $\nu = 125.8$ MHz.

the Cu^{II} exchange is very slow and that the peaks observed belong to the apo form of the peptide, with those of the Cu^{II} complex being fully broadened and thus difficult to detect, which is in line with what was proposed on longer HSA N-terminal fragments.[19] This hypothesis is confirmed by quantification of the ^1H NMR spectroscopic signal, which shows that in presence of 0.5 equiv of Cu^{II}, the intensity of the signal recorded is about half that of the apopeptide (Figure S6 in the Supporting Information). Knowing that the Cu^{II} binding affinities for both peptides are close,[2b,20] this result was unanticipated. Actually, the reason for such a discrepancy may be connected to the fact that, in a substoichiometric Cu^{II} ratio, GHK can form $[Cu^{II}(GHK)_2]$ species (see

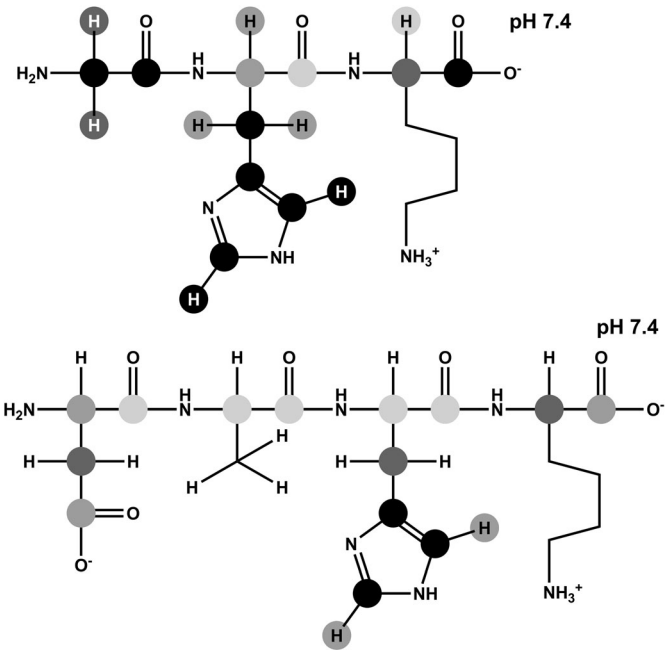

Scheme 1. Schematic representation of the C and H atoms for which the NMR spectroscopic signal is broadened upon addition of Cu^{II} to GHK (top) and DAHK (bottom) at pH 7.2. Black = highly broadened, dark grey = broadened, grey = moderately broadened, light grey = slightly broadened.

Figure S7 in the Supporting Information and ref. [2b]), with the second GHK occupying the fourth equatorial position through the imidazole ring of the His side chain (see the EPR spectrum in Figure 5 and ref. [21]). Formation of such a ternary complex will help Cu exchange from one peptide to another. As previously described,[14e] Cu^{II} broadening of peptide residues can also originate from involvement in Cu transfer (even if the Cu transfer is very slow, as in the case of DAHK). This is one possible reason why Asp and His lateral chains and the C- and N-terminal of DAHK are the residues mostly affected. The second possibility is that these four functions (from the apo peptide) may be involved in chemical exchange for Cu^{II} apical binding (in the holo peptide). Related to that, the carboxylate groups from Asp1 or C-terminal are equivalently broadened, which strongly suggests that these functions are involved in Cu transfer but not in direct Cu binding in solution. Hence, this data is in disagreement with the previously proposed coordination of Asp1 carboxylate function in the Cu^{II} apical position.[12]

Electrochemistry: Cyclic voltammetry (CV) traces of $[Cu^{II}(GHK)]$ and $[Cu^{II}(DAHK)]$ complexes are shown in Figure 9. The main difference with previous data published in the literature is the nature of the working electrode.[22] In the present study, we used vitreous carbon electrode, which has been shown to be a well-suited surface for the study of Cu^{II}–peptide complexes.[23]

The CV trace of the $[Cu^{II}(DAHK)]$ complex shows no cathodic process and a reversible anodic process at $E^{1/2} =$

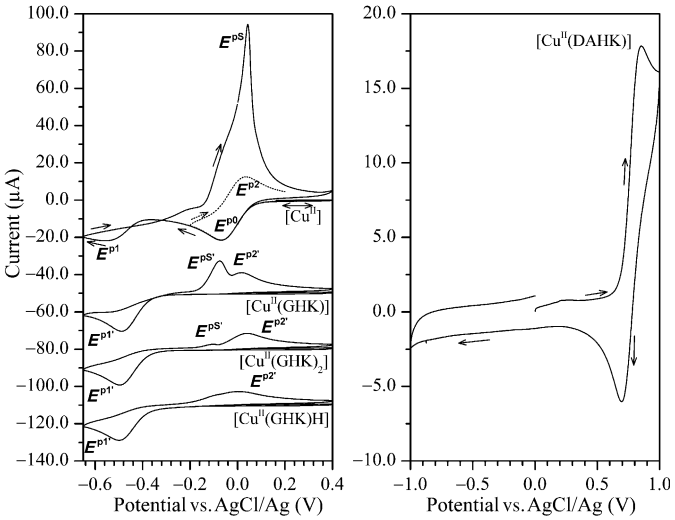

Figure 9. Cyclovoltammogram recorded for $[Cu^{II}]$, $[Cu^{II}(GHK)]$, $[Cu^{II}(GHK)_2]$, $[Cu^{II}(GHK)H]$ (left panel) and for $[Cu^{II}(DAHK)]$ (right panel). Experimental conditions: scan rate 100 mV s^{-1}, $T = 298$ K, 0.1 M 50 mM, Tris buffer pH 7.4, 0.1 M $NaClO_4$, $[Cu^{II}(DAHK)] = 2$ mM; $[Cu^{II}(GHK)] = 1.6$ mM.

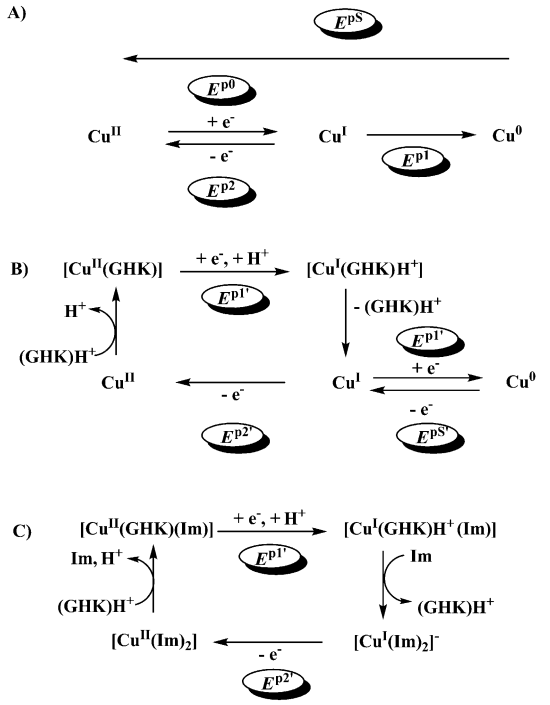

Scheme 2. Electrochemical processes associated with the reduction of A) $[Cu^{II}]$, B) of the $[Cu^{II}(GHK)]$ complex and C) of the $[Cu^{II}(GHK)]$ complex in presence of an imidazole (Im) donor species. Potentials refer to Figure 9.

0.77 V versus AgCl/Ag ($\Delta E^p = 130$ mV) that corresponds to the reversible oxidation of the $[Cu^{II}(DAHK)]$ complex into $[Cu^{III}(DAHK)]^+$, which is in line with what was previously observed for related complexes.[24] More precisely, the $E^{1/2}$ oxidation process abides by the following trend with respect to the equatorial binding plane: $\{NH_2, 3N^-\}$[24a] (0.41 V versus AgCl/Ag) < $\{Im(His), 3N^-\}$[24b] (0.66 V versus AgCl/Ag) < $\{NH_2, Im(His), 2N^-\}$ (0.77 V versus AgCl/Ag).

The CV trace of the $[Cu^{II}(GHK)]$ complex shows no anodic process and an irreversible cathodic process at $E^{p1} = -0.49$ V versus AgCl/Ag that corresponds to the reduction of the $[Cu^{II}(GHK)]$ complex. This is in drastic contrast to the CV trace obtained for Cu^{II} with no peptide in the same buffer, which shows a reduction of Cu^{II} to Cu^{I} at $E^{p0} = -0.07$ V versus AgCl/Ag followed by reduction of Cu^{I} to Cu^0 at $E^{p1} = -0.54$ V versus AgCl/Ag (redox processes are summarised in Scheme 2A). On the reverse scan for $[Cu^{II}(GHK)]$, a first anodic peak is detected at $E^{pS'} = -0.07$ V versus AgCl/Ag. Its shape and position are characteristic of the oxidation–solubilisation process of adsorbed Cu^0 that lead to Cu^{I}. A second anodic peak is detected at $E^{p2'} = 0.02$ V versus AgCl/Ag and corresponds to oxidation of Cu^{I} to Cu^{II}. This indicates that reduction of $[Cu^{II}(GHK)]$ is followed by decoordination of the peptide ligand. Due to the difference in Lewis acidity of Cu^{I} and Cu^{II}, protonation of the amidyl function of the Gly–His peptide bond involved in the Cu^{II} binding is likely concomitant with the reduction process. At the $[Cu^{II}(GHK)]$ reduction potential (−0.54 V versus AgCl/Ag), unbound Cu^{I} is reduced to Cu^0[25] and adsorbed onto the electrode. When scanning back towards cathodic potential, the reduction of unbound Cu^{II} to Cu^{I} (expected near $E^{p0} = -0.07$ V versus AgCl/Ag) is not observed, thus indicating that formation of the $[Cu^{II}(GHK)]$ complex is faster than 1 s. The different redox processes detected in the CV trace of the $[Cu^{II}(GHK)]$ complex are summarised in Scheme 2B.

In the presence of an excess amount of GHK or His, the cathodic peak is not modified significantly, which means that the nature (N or O) of the fourth ligand has little impact on the reduction process. On the contrary, the desorption peak (p2 in Figure 9) is greatly reduced and the oxidation peak of Cu^{I} to Cu^{II} ($E^{p2'}$) is slightly shifted. This is in line with the coordination of Cu^{I} by the imidazole (Im) from the side chain of GHK or His. We propose that in the presence of an excess amount of GHK or His, the Cu^{I} release after reduction of the $[Cu^{II}(GHK)]$ species is coordinated by the excess ligand, thus leading to the formation of a new Cu^{I} complex. This new Cu^{I} complex is oxidised at $E^{p2'} = 0.04$ V versus AgCl/Ag (in the case of an excess amount of GHK) and $E^{p2'} = -0.01$ V versus AgCl/Ag (in the case of an excess amount of His). In this latter case, we propose that the motif Im-Cu^{I}-Im, which is quite usual in Cu^{I} coordination,[26a,b] is formed (illustrated in Scheme 2C). In the former case, the GHK ligand may remain bound by both the terminal $-NH_2$ and the His.

Note that we also performed the same series of experiments in phosphate buffer (see Figure S8 and Scheme S2 in the Supporting Information). In the latter case, it is not possible to record the CV trace of unbound Cu^{II} because of its rapid precipitation in phosphate buffer. However, in the presence of GHK or DAHK peptide, the results obtained in phosphate buffer were fully consistent with those obtained

in tris(hydroxymethyl)aminomethane (Tris) buffer except for small modifications in peak potentials. This suggests that, even if the tris buffer interferes with Cu^{II} binding to DAHK and GHK peptides, this doesn't impact significantly the electrochemical signatures.

Reactive oxygen species (ROS) production: The cyclic voltammetry data of the [Cu^{II}(GHK)] complex provide evidence of an irreversible reduction peak at −0.62 V versus AgCl/Ag, whereas those of the [Cu^{II}(DAHK)] show a unique reversible oxidation process at 0.72 V versus AgCl/Ag (but no reduction process); hence these data suggest the impossibility for both complexes to be directly reduced by ascorbate (Asc). This is why catalytic oxidation of Asc under aerobic conditions by both complexes was compared to oxidation by unbound Cu^{II}. Consumption of Asc was monitored by the decrease of its absorption band at 265 nm. Drastic deceleration of Asc consumption was observed in the presence of both peptides (Figure S9 in the Supporting Information), which is in line with a redox silencing of Cu^{II} when bound to the peptides and with the redox potential values of the [Cu^{II}(GHK)] and [Cu^{II}(DAHK)] complexes and that of Asc ($\approx$0.1 V versus AgCl/Ag).

Previous results showed a propensity of the [Cu^{II}(GHK)] complex to catalyze the $HO^{\bullet}$ formation using Asc as reductant.[22b] As $HO^{\bullet}$ production from dioxygen requires the redox cycling of the copper complex (Scheme S3 in the Supporting Information), and as our data show that Asc is unable to reduce [Cu^{II}(GHK)], these results were re-evaluated. Fluorescence measurements were performed by using coumarin-3-carboxylic acid. We found very weak $HO^{\bullet}$ production (in the range of residual $HO^{\bullet}$ production in the absence of added Cu^{II} ion) for both [Cu^{II}(GHK)] and [Cu^{II}(DAHK)] complexes relative to the $HO^{\bullet}$ production in similar concentrations of unbound Cu^{II} (Figure S10 in the Supporting Information). Similar results were obtained with EPR using the α-(4-pyridyl-1-oxide)-*N*-*tert*-butylnitrone (POBN) spin trap (data not shown). Error in the previous results[22b] with regards to the [Cu^{II}(GHK)] complex is attributed either to 1) a miscalculation of the GHK concentration (see the Experimental Section), thus leading to unbound Cu^{II} in solution or 2) an inversion with data of the [$Cu^{II}(Gly)_2$] species, which was found to produce no $HO^{\bullet}$,[22b] a result further questioned.[27]

Conclusion

In the present work we gained new insight into the structural aspects of [Cu^{II}(GHK)] and [Cu^{II}(DAHK)] and reported data on their redox behaviour. The use of several spectroscopic techniques together with the determination of the crystal structure gave a complete set of information, which will be important as reference in the analysis of other, more complicated Cu^{II}–peptide interactions with peptides such as amyloid-β or α-synuclein sequences, for example, for which no crystal structure is available. Moreover, the analysis shed new light on Cu^{II} exchange dynamics and redox behaviour in particular. This is important in the biological context. DAHK is the high-affinity Cu^{II} binding site of human serum albumin; this region is 5% occupied with Cu^{II}. This is the first time this copper-loaded sequence has been crystallised. It has been suggested that albumin is involved in Cu^{II} transport in the blood towards other targets. The slow exchange rate of Cu^{II} in DAHK indicates that albumin is not a fast Cu^{II} supplier. The observation of an axial water molecule indicates that also other ligands can bind on this labile position, which might be the reason why Cu^{II} is not completely inert and can be exchanged, albeit very slowly. Thus differences in the coordination of the apical position might explain differences seen between the reactivity of [Cu^{II}-(DAHK)] and Cu–albumin.[8,28] Although the affinity of GHK for Cu^{II} is on the same order of magnitude as that of DAHK,[21] it exchanges much faster and hence could serve as a fast Cu^{II} supplier. The structural reason for that is that the fourth equatorial binding site on Cu^{II} is available to bind a transfer partner. Another way to transfer Cu^{II} from DAHK and GHK is by reducing Cu^{II} to Cu^{I}, which might occur in the reducing intracellular environment. The CV results indicate that Cu^{II} in DAHK is stable and not reduced to Cu^{I}. By contrast, it is possible in the case of GHK with a concomitant release of Cu^{I}. Thus Cu^{II} in GHK could be released and transferred to other targets by reduction (with reductants stronger than Asc), as it could be expected intracellularly.

Experimental Section

Chemicals: All solutions were prepared with Milli-Q (18 MΩ) water. GHK peptide was bought from Bachem (Switzerland); DAHK peptide was bought from Bachem (Switzerland) or GeneCust (Dudelange, Luxembourg). pH was controlled using a 744 pH meter equipped with a biotrode electrode (Metrohm SA, Switzerland). Stock solutions of peptides were prepared by dissolving the peptides in D_2O ($\approx$50 mg in 1 mL) and concentrations were determined by titration followed by UV/Vis absorption spectroscopy (using an Agilent 8453 spectrometer at 25 °C in 1 cm path-length quartz cuvette). In a typical experiment, the stock solution was diluted tenfold and amounts of a Cu^{II} solution of known concentration were added until no increase in the d–d band of the Cu^{II}–peptide complex and turbidimetry due to unbound Cu^{II} precipitation in the buffer were observed. Measurements were performed in 0.1 M phosphate buffer (pH 7.4). This experimental determination led to concentration values that are 10–20% off compared to those obtained using the molecular mass of the peptide and its counterions, thereby suggesting that counterion salts co-precipitate during peptide synthesis. Stock solutions were stored at −20 °C. Unless specified, the Cu^{II} ion source was hydrated $Cu(SO_4)$. For EPR measurements, a 0.1 M stock solution of $^{63}Cu(NO_3)_2$ obtained by nitric acid treatment of isotopically pure ^{63}Cu (Eurisotop, Saclay, France) was used and 10% glycerol was added to the samples. [$Cu(GHK)_2$], [Cu(GHK)H] and [Cu(GHK)G] were prepared by adding GHK (1 equiv), His (1 equiv) and Gly (10 equiv) to the [Cu(GHK)] complex, respectively.

For ascorbate, a stock solution (20 mM) of ascorbate was prepared in milli-Q water at room temperature just before beginning the experiment and was used immediately. Because ascorbate degrades very quickly, a new solution was prepared for each experiment.

A stock solution (1 mM) of desferrioxamine (DFO, Sigma) was prepared by dissolving the appropriate mass in milli-Q water.

A stock solution of coumarin-3-carboxylic acid (5 mM) was prepared in phosphate (20 mM), NaCl (100 mM) buffer at pH 9 at room temperature. The stock solution was stored at −20 °C.

^{15}N-labelled glycine, ^{13}C-(COO^-)-labelled glycine and ^{15}N(Im)-labelled histidine were purchased from Eurisotop (Saclay, France).

X-ray diffraction: Crystals suitable for X-ray diffraction were obtained by slow ethanol diffusion and evaporation of a 0.2 M solution in milli-Q water of the corresponding complex. Data were collected using a Kappa X8 APPEX II Bruker diffractometer with graphite-monochromated $Mo_{K\alpha}$ radiation ($\lambda = 0.71073$ Å). The temperature of the crystal was maintained at the selected value (100 K) by using a 700 series Cryostream cooling device within an accuracy of ±1 K. Intensity data were corrected for Lorentz polarisation and absorption factors. The structures were solved by direct methods using SHELXS-97[29] and refined against F^2 by full-matrix least-squares techniques using SHELXL-97[30] with anisotropic displacement parameters for all non-hydrogen atoms.

Treatment of H: H atoms of the ligand were added from the difference Fourier map and refined by the riding model. For the [Cu^{II}(DAHK)] complex only, the H atoms of the water molecules were subsequently included in the refinement in geometrically idealized positions, with C–H = 0.96(3) Å and H–H = 1.52(3) Å, and refined using the riding model with isotropic displacement parameters of $U_{iso}(H) = 1.4\,U_{eq}$ (parent atom). For [Cu^{II}(GHK)], the lateral chain of lysine is disordered over two sites with occupancies of 0.5:0.5. Occupancy parameters for the 16 water oxygen atoms were refined. The net occupancy of the ordered water is 9.25. All calculations were performed by using the Crystal Structure crystallographic software package WINGX.[31] The absolute configuration was determined by refining the Flack parameter[32] using a large number of Friedel pairs.

CCDC-809108 ([Cu^{II}(GHK)]) and 809109 ([Cu^{II}(DAHK)]) contain the supplementary crystallographic data for this paper. These data can be obtained free of charge from The Cambridge Crystallographic Data Centre via www.ccdc.cam.ac.uk/data_request/cif.

ESI-MS measurements: ESI mass spectra were recorded using an API 365 MS mass spectrometer at a flow rate of 5 μL min^{-1}.

XAS measurements: Cu K-edge XAS spectra were recorded using the SAMBA bending magnet beamline at Synchrotron SOLEIL (Saint-Aubin, France). The main optical elements consisted of a double crystal Si(111) dynamical focusing monochromator between two palladium-coated mirrors, one collimating the beam in the vertical direction and one focusing it on the sample. X-ray harmonic rejection was obtained by setting the energy cutoff to change the incidence of the mirrors. The measurements were performed on solution samples at room temperature in the fluorescence mode using a single-element Silicon Drift Detector (SDD). The energy was calibrated by the simultaneous measurement of a Cu foil spectrum in transmission (first inflection point set at 8980.3 eV). Possible X-ray photo-reduction of the [Cu^{II}(peptide)] samples was monitored by checking, on consecutive scans, the appearance of the XANES feature at 8984 eV, which is typical of Cu^I formation. After 5 scans, which lasted around 10 min each, the feature was still small, thus indicating a poor reduction effect. Two series of around 10 to 20 scans were recorded. For the EXAFS analysis, the photo-reduction of scans that can be neglected was averaged. For the XANES study, only the two first scans of each series were added. Points were measured every 0.25 eV in the XANES region and steps were gradually increased from 0.5 eV (at E = 9000 eV) to 5 eV (at E = 9600 eV) in the EXAFS region.

EPR spectroscopy: EPR spectra (9.4 GHz) were recorded using a Bruker ELEXSYS 500 spectrometer equipped with a continuous-flow He cryostat (Oxford). The field modulation frequency was 100 kHz. Pulsed EPR experiments were recorded using a Bruker ELEXSYS 580 spectrometer at liquid helium temperatures. Pulsed EPR data were processed by using routines locally written with Matlab (R2008b, The Mathworks, Inc.).

NMR spectroscopy: 1D ^1H and ^{13}C experiments and 2D experiments were recorded using a Bruker Avance 500 spectrometer equipped with a 5 mm triple-resonance inverse Z-gradient probe (TBI ^1H, ^{31}P, BB). All chemical shifts are relative to tetramethylsilane. 1D NMR and 2D NMR spectra were collected at 298 K in pure D_2O.

Cyclic voltammetry (CV): CV measurements were recorded under argon using a 620C electrochemical analyzer (CH Instruments, Inc). The working electrode was a glassy carbon disk and a Pt wire was used as counter-electrode. The reference electrode was an AgCl/Ag electrode (0.223 V versus NHE) isolated in a fritted bridge. Immediately before the measurement of each voltammogram, the working electrode was carefully polished with alumina suspensions (1, 0.3 and 0.05 μm, successively), sonicated in an ethanol bath and then washed carefully with ethanol. The electrochemical cell medium used was milli-Q water with 0.1 M sodium phosphate (pH 7.4) added as supporting electrolyte.

Measurements of $HO^\bullet$ production: These were performed in phosphate (20 mM), NaCl (100 mM) buffer at pH 7.4. The reaction was started by the addition of ascorbate (500 μM). In all these experiments, DFO (at a final concentration of 1 or 2 μM depending on buffer concentration) was added to avoid non-specific $OH^\bullet$ production by metallic ion impurities from the buffer.

Coumarin-3-carboxylic acid (3-CCA) (Sigma) was used to detect $HO^\bullet$.[22b] $HO^\bullet$ reacts with 3-CCA to form 7-hydroxycoumarin-3-carboxylic acid (7-OH-CCA), which is fluorescent at 452 nm upon excitation at 395 nm. The intensity of the fluorescence signal is proportional to the number of 7-OH-CCA molecules formed, which in turn is proportional to the $HO^\bullet$ radicals generated. [CCA] = 500 μM.

Ascorbate consumption was monitored by UV/Vis spectroscopy. The intensity of the Asc absorption band at $\lambda = 265$ nm ($\varepsilon = 14\,500$ M^{-1}cm^{-1}) was monitored as a function of time, in 100 mM phosphate buffer (pH 7.4) that contained 100 μM of Asc, 2 μM of DFO, 5 μM of Cu^{II} and after addition of 6 μM of GHK or DAHK peptide.

Acknowledgements

This work was supported by a grant from the Agence Nationale de la Recherche, Programme Blanc NT09-488591, "NEUROMETALS" (P.F., C.H. and P.D.) and 05-JCJC-0010-01, "NEUROARPE" (P.D.). We thank the staff of the SAMBA beamline at SOLEIL and more particularly Dr. Emiliano Fonda for help in performing the XAS experiments (SOLEIL Project 20080324). Dr. Yannick Coppel and Valérie Bourdon are acknowledged for their help in NMR spectroscopic experiments and analysis and in ESI-MS experiments, respectively. We thank Fanny Leroux for earlier results obtained on [Cu^{II}(GHK)], Bertrand Badei for the ascorbate consumption experiments and Bruno Alies for his participation in the NMR spectroscopic experiments.

[1] a) H. Kozlowski, A. Janicka-Klos, J. Brasun, E. Gaggelli, D. Valensin, G. Valensin, *Coord. Chem. Rev.* **2009**, *253*, 2665–2685; b) E. Gaggelli, H. Kozlowski, D. Valensin, G. Valensin, *Chem. Rev.* **2006**, *106*, 1995–2044.

[2] a) C. Harford, B. Sarkar, *Acc. Chem. Res.* **1997**, *30*, 123–130; b) C. Conato, R. Gavioli, R. Guerrini, H. Kozlowski, P. Mlynarz, C. Pasti, F. Pulidori, M. Remelli, *Biochim. Biophys. Acta Gen. Subj.* **2001**, *1526*, 199–210; c) M. Rózga, M. Sokolowska, A. M. Protas, W. Bal, *J. Biol. Inorg. Chem.* **2007**, *12*, 913–918.

[3] L. Pickart, M. M. Thaler, *Nature* **1973**, *243*, 85–87.

[4] A. Siméon, F. Monier, H. Emonard, Y. Wegrowski, G. Bellon, J. C. Monboisse, P. Gillery, W. Hornebeck, F.-X. Maquart, *Curr. Top. Pathol.* **1999**, *93*, 95–101.

[5] L. Pickart, *J. Biomater. Sci. Polym. Ed.* **2008**, *19*, 969–988.

[6] P. M. May, J. Whittaker, D. R. Williams, *Inorg. Chim. Acta* **1983**, *80*, L5–L7.

[7] D. C. Carter, J. X. Ho, *Adv. Protein Chem.* **1994**, *45*, 153–203.

[8] W. Bal, J. Christodoulou, P. J. Sadler, A. Tucker, *J. Inorg. Biochem.* **1998**, *70*, 33–39.

[9] C. M. Perkins, N. J. Rose, B. Weinstein, R. E. Stenkamp, L. H. Jensen, L. Pickart, *Inorg. Chim. Acta* **1984**, *82*, 93–99.

[10] J. F. Blount, K. A. Fraser, J. T. Freeman, J. T. Szymanski, C.-H. Wang, *Acta Crystallogr.* **1967**, *22*, 396–405.
[11] N. Camerman, A. Camerman, B. Sarkar, *Can. J. Chem.* **1976**, *54*, 1309–1316.
[12] J. P. Laussac, B. Sarkar, *J. Biol. Chem.* **1980**, *255*, 7563–7568.
[13] M. Sano, S. Komorita, H. Yamatera, *Inorg. Chem.* **1992**, *31*, 459–463.
[14] a) V. A. Streltsov, S. J. Titmuss, V. C. Epa, K. J. Barnham, C. L. Masters, J. N. Varghese, *Biophys. J.* **2008**, *95*, 3447–3456; b) R. W. Strange, L. Alagna, P. Durham, S. S. Hasnain, *J. Am. Chem. Soc.* **1990**, *112*, 4265–4268; c) P. Frank, M. Benfatto, B. Hedman, K. O. Hodgson, *Inorg. Chem.* **2008**, *47*, 4126–4139; d) E. Borghi, P. L. Solari, *J. Synchrotron Radiat.* **2005**, *12*, 102–110; e) C. Hureau, Y. Coppel, P. Dorlet, P. L. Solari, S. Sayen, E. Guillon, L. Sabater, P. Faller, *Angew. Chem.* **2009**, *121*, 9686–9689; *Angew. Chem. Int. Ed.* **2009**, *48*, 9522–9525.
[15] a) J. H. Freedman, L. Pickart, B. Weinstein, W. B. Mims, J. Peisach, *Biochemistry* **1982**, *21*, 4540–4544; b) G. Rakhit, B. Sarkar, *J. Inorg. Biochem.* **1981**, *15*, 233–241.
[16] J. Peisach, W. E. Blumberg, *Arch. Biochem. Biophys.* **1974**, *165*, 691–708.
[17] a) S. Stoll, C. Calle, G. Mitrikas, A. Schweiger, *J. Magn. Reson.* **2005**, *177*, 93–101; b) B. Kasumaj, S. Stoll, *J. Magn. Reson.* **2008**, *190*, 233–247; c) P. Dorlet, S. Gambarelli, P. Faller, C. Hureau, *Angew. Chem.* **2009**, *121*, 9437–9440; *Angew. Chem. Int. Ed.* **2009**, *48*, 9273–9276.
[18] I. Bertini, C. Luchinat, *Coord. Chem. Rev.* **1996**, *150*, 77–110.
[19] J. P. Laussac, B. Sarkar, *Biochemistry* **1984**, *23*, 2832–2838.
[20] M. Sokolowska, A. Krezel, M. Dyba, Z. Szewczuk, W. Bal, *Eur. J. Biochem.* **2002**, *269*, 1323–1331.
[21] A. Trapaidze, C. Hureau, W. Bal, M. Winterhalter, P. Faller, unpublished results.
[22] a) K. Takehara, Y. Ide, *Inorg. Chim. Acta* **1991**, *183*, 195–202; b) L. Guilloreau, S. Combalbert, A. Sournia-Saquet, H. Marzaguil, P. Faller, *ChemBioChem* **2007**, *8*, 1317–1325.
[23] V. Balland, C. Hureau, J.-M. Savéant, *Proc. Natl. Acad. Sci. USA* **2010**, *107*, 3367–3372.
[24] a) D. W. Margerum, K. L. Chellappa, F. P. Bossu, G. L. Burce, *J. Am. Chem. Soc.* **1975**, *97*, 6874–6876; b) C. Hureau, L. Charlet, P. Dorlet, F. Gonnet, L. Spadini, E. Anxolabéhère-Mallart, J.-J. Girerd, *J. Biol. Inorg. Chem.* **2006**, *11*, 735–744.
[25] M. Brzyska, K. Trzesniewska, A. Wieckowska, A. Szczepankiewicz, D. Elbaum, *ChemBioChem* **2009**, *10*, 1–12.
[26] a) S. Furlan, C. Hureau, P. Faller, G. La Penna, *J. Phys. Chem. B* **2010**, *114*, 15119–15133; b) C. Hureau, V. Balland, Y. Coppel, P. L. Solari, E. Fonda, P. Faller, *J. Biol. Inorg. Chem.* **2009**, *14*, 995–1000.
[27] R. C. Nadal, S. E. Rigby, J. H. Viles, *Biochemistry* **2008**, *47*, 11653–11664.
[28] L. Perrone, E. Mothes, M. Vignes, A. Mockel, C. Figueroa, M. C. Miquel, M. L. Maddelein, P. Faller, *ChemBioChem* **2010**, *11*, 110–118.
[29] SHELXS-97, Program for Crystal Structure Solution, G. M. Sheldrick, University of Göttingen, Göttingen (Germany), **1997**.
[30] SHELXL-97, Program for the refinement of crystal structures from diffraction data, G. M. Sheldrick, University of Göttingen, Göttingen (Germany), **1997**.
[31] L. J. Farrugia, *J. Appl. Crystallogr.* **1999**, *32*, 837–838.
[32] H. D. Flack, *Acta Crystallogr. Sect. A* **1983**, *39*, 876–881.

Received: March 11, 2011
Published online: July 20, 2011

